Mechanism of Antibacterial Action of Dermaseptin B2: Interplay between Helix−Hinge−Helix Structure and Membrane Curvature Strain[†]

Cécile Galanth,*[,‡] Feten Abbassi,[‡] Olivier Lequin,[§] Jésus Ayala-Sanmartin,[||] Ali Ladram,[‡] Pierre Nicolas,[‡] and Mohamed Amiche*[,‡]

Peptidome de la Peau des Amphibiens, UPMC Université Paris 06, CNRS FRE 2852, F-75005 Paris, France, Synthèses, Structure et Fonction de Molécules Bioactives, UPMC Université Paris 06, CNRS UMR 7613, F-75005 Paris, France, and INSERM UMRS893, UPMC Université Paris 06, CdR Saint Antoine, F-75012 Paris, France

Received October 30, 2008; Revised Manuscript Received November 28, 2008

ABSTRACT: Dermaseptin B2 (Drs B2) is a 33-residue-long cationic, α-helical antimicrobial peptide endowed with membrane-damaging activity against a broad spectrum of microorganisms, including bacteria, yeasts, fungi, and protozoa, but its precise mechanism of action remained ill-defined. A detailed characterization of peptide−membrane interactions of Drs B2 was undertaken in comparison with a C-terminal truncated analogue, [1−23]-Drs B2, that was virtually inactive on bacteria despite retaining the cationic charge of the full-length peptide. Both peptides were tested on living cells using membrane permeabilization assays and on large unilamellar and multilamellar phospholipid vesicles composed of binary lipid mixtures by dye leakage assay, fluorescence spectroscopy, circular dichroism, and differential scanning calorimetry and also on SDS micelles using NMR spectroscopy. The results indicate that Drs B2 induces a strong perturbation of anionic lipid bilayers, resides at the hydrocarbon core−water interface, parallel to the plane of the membrane, and interacts preferentially with the polar head groups and glycerol backbone region of the anionic phospholipids, as well as the region of the lipid acyl chain near the bilayer surface. The interfacial location of Drs B2 induces a positive curvature of the bilayer and clustering of anionic lipids, consistent with a carpet mechanism, that may lead to the formation of mixed peptide−phospholipid toroidal, transient pores and membrane permeation/disruption once a threshold peptide accumulation is reached. In constrast, the truncated [1−23]-Drs B2 analogue interacts at the head group level without penetrating and perturbing the hydrophobic core of the bilayer. NMR study in SDS micelles showed that [1−23]-Drs B2 adopts a well-defined helix encompassing residues 2−20, whereas Drs B2 was previously found to adopt helical structures interrupted around the Val^{9}-Gly^{10} segment. Thus the antibacterial activity of Drs B2 depends markedly on a threshold number of hydrophobic residues to be present on both extremities of the helix. In a membrane environment with a strong positive curvature strain, Drs B2 can adopt a flexible helix−hinge−helix structure that facilitates the concomitant insertion of the strongly hydrophobic N- and C-termini of the peptide into the acyl core of the membrane.

Despite the growing interest in the use of cationic antimicrobial peptides (AMPs)[1] as a potential source of novel antibiotics, there are but rare instances of rational designs of highly potent and selective AMP analogues that can be manufactured as antibiotics at competitive costs for therapeutic use (*1*−*6*). Known naturally occurring AMPs differ dramatically in size (from ∼10 to 50 residues), sequence, and three-dimensional structure and share net positive charge and amphipathicity (*7*). Many of them adopt an α-helical amphipathic structure in membrane environments, which is considered to be a prerequisite for their lytic activity (*8*−*12*). Several in vitro and in vivo studies have demonstrated that antimicrobial activity is mediated by a complex, sensitive balance between various peptide parameters, including the length, net charge, hydrophobicity, secondary structure propensity, amphipathicity, size and depth of the helical polar/apolar sectors, flexibility, and resistance to degradation, and that the role of each parameter may change from one peptide to another (*4, 6, 13*−*19*). Thus, engineering peptides with low toxicity and high antimicrobial activity is actually restricted to a case-by-case study. Moreover, although it is

[†] This work was supported by grants from the Centre National de la Recherche Scientifique (CNRS) and the Agence Nationale pour la Recherche (ANR-Prob DOM).

* Address correspondence to these authors. C.G.: phone, +33-144275686; fax, +33-144275994; e-mail, cecile.galanth@etu.upmc.fr. M.A.: phone, +33-144275686; fax, +33-144275994; e-mail, mohamed.amiche@upmc.fr.

[‡] UPMC Université Paris 06, CNRS FRE 2852.

[§] UPMC Université Paris 06, CNRS UMR 7613.

[||] INSERM UMRS893, UPMC Université Paris 06.

[1] Abbreviations: AMP, antimicrobial peptide; CD, circular dichroism; CSD, chemical shift deviation; DiPoPE, 1,2-dipalmitoleoyl-*sn*-glycero-3-phosphocholine; DMPC, 1,2-dimyristoyl-*sn*-glycero-3-phosphocholine; DMPE, 1,2-dimyristoyl-*sn*-glycero-3-phosphoethanolamine; DMPG, 1,2-dimyristoyl-*sn*-glycero-3-[phospho-(1-glycerol)]; Drs, dermaseptin; DSC, differential scanning calorimetry; HSQC, heteronuclear single-quantum correlation; LUV, large unilamellar vesicles; MIC, minimal inhibitory concentration; MLVs, multilamellar vesicles; NMR, nuclear magnetic resonance; NOE, nuclear Overhauser effect; NOESY, NOE spectroscopy; ONPG, *o*-nitrophenyl β-D-galactopyranoside; PBS, phosphate-buffered saline; SDS, sodium dodecyl sulfate; TFE, trifluoroethanol; TOCSY, total correlation spectroscopy.

10.1021/bi802025a CCC: $40.75
Published on Web 12/29/2008

well established that AMPs kill microbial cells by compromising the structural and functional integrity of the lipid plasma bilayer of the target cells, their detailed mechanism of action as well as the molecular basis of their microbial membrane selectivity are still ill-defined (*11, 20*−*22*). There are currently two major models for the mechanism of action of linear cationic AMPs on lipid bilayer membranes. The barrel−stave model predicts membrane permeation through peptide aggregation on or within the membrane to form water-filled pores lined with the polar face of the peptide (*23*). In the carpet model, the cationic peptide binds to the surface of the bilayer, parallel to the membrane plane, with the hydrophobic amino acids penetrating partly into the bilayer hydrocarbon core and the cationic residues interacting with the negatively charged phosphate moieties of the lipid head groups. A fraction of the peptide lying parallel to the plane of the membrane may change its orientation from parallel to transversal, promoting a positive curvature of the membrane and forming mixed phospholipid−peptide toroidal pores that permabilize the membrane. This may eventually lead to the disruption/solubilization of the membrane in a detergent-like manner once a threshold concentration is reached (*24*−*31*).

Sequence shortening of AMPs while retaining specificity and activity is a major prerequisite in the therapeutic development of AMPs in order to produce large quantities of peptide at competitive costs and to enhance biodisposability. A representative example in this direction is the systematic truncation of the dermaseptins, a family of closely related linear, cationic antimicrobial peptides from frog skin that have 24−34 residues (*32, 33*). Dermaseptin S1 (Drs S1), a 34-residue peptide, exerts a lytic action upon bacteria, protozoa, yeasts, and filamentous fungi at micromolar concentrations, without harmful effect on differentiated mammalian cells (*34*). Shortening the peptide chain of Drs S1 to [1−18]-Drs S1 yielded a peptide exhibiting enhanced antimicrobial potency, yet displaying even less in vitro toxicity compared with Drs S1 (*34, 35*). Shortening the peptide chain of dermaseptin S3 (30 residues) to [1−16]-Drs S3 did not affect the antimicrobial potency of the peptide. Analogues of Drs S3 10−12 residues in length remained fully active against *Enterococcus faecalis*, *Cryptococcus neoformans*, and *Aeromonas caviae*, the causal agent of red-leg disease in amphibians (*36*). From the initial 28-residue Drs S4, a tridecapeptide K4[1−13]-Drs S4 with a 30-fold decrease in cytotoxicity was derived, with leishmanicidal and antiplasmodial activities decreased less than one log order (*37, 38*). One may thus ask how peptides as short as [1−10]-Drs S3 retain antimicrobial activity relative to the parent molecules and which is (are) the role(s) of the remainder of the residues of the peptide?

However, the detailed mechanism of dermaseptin membrane permeation, both from peptide and lipid perspectives, has not yet been provided. Data using simple artificial membranes and/or molecular dynamic simulations (*39*) led to the proposal that the dermaseptins bind to and permeate microbial cells through a carpet-like mechanism of action and that the N-terminal region of these peptides is mainly responsible for their membrane effects (*24, 34, 35, 40*). Planar lipid bilayers studies suggested that Drs B2 is able to form mixed lipid−peptide pores mainly formed by Drs tetramers (i.e., toroidal pores) (*41*). Moreover, the relationship between the three-dimensional structure of the membrane-bound dermaseptins and the proposed mechanism of membrane-perturbing action remains elusive. For instance, NMR studies showed that Drs B2 adopts different α-helical structures depending on the environment (TFE/water mixture or SDS micelles) (*42*). In contrast, Drs S3 does not adopt an α-helical structure in TFE/water but has several turn-like regions along the polypeptide chain (*43*). Drs S4, which has weak antibacterial activity but potent hemolytic and antiprotozoan effects, was found to be highly aggregated in aqueous solution through hydrophobic interactions involving the N-terminal region, thus preventing NMR analysis (*44*). Finally, a current working hypothesis is that antimicrobial peptides may recruit specific lipids from the membrane leading to the formation of lipid microdomains possessing specific physicochemical properties that will trigger the peptide biological activity on the membrane (*45*). This hypothesis has not been evaluated by the above approaches that have been conducted on rather simple model systems, mainly composed of a single lipid species.

Thus, a unifying model that correlates the structural and physicochemical parameters of dermaseptins with their antibacterial properties is still lacking, and a case-by-case systematic characterization of peptide−membrane interactions, including peptide secondary and tertiary structure determination, and of lipid membrane perturbation and supramolecular organization is essential to determine the precise molecular mechanism of dermaseptin action. To address these issues, we synthesized a truncated analogue of Drs B2, [1−23]-Drs B2, that lacks the C-terminal 24−33 hydrophobic segment devoid of the parent peptide. Unexpectedly, the C-terminally truncated analogue was virtually inactive on all tested microorganisms while retaining the cationic charge of DrsB2. This poorly active analogue represented therefore a good model to be compared with full-length DrsB2, in order to pinpoint the critical structural and membrane interaction properties of DrsB2 that are involved in cell membrane lysis. The comparative analysis of Drs B2 and [1−23]-Drs B2 was undertaken on living cells using a bacterial permeation assay, on LUVs and MLVs composed of binary lipid mixtures as models for prokaryotic and eukaryotic plasma membranes using several biophysical techniques, fluorescence spectroscopy, circular dichroism, and differential scanning calorimetry, and on detergent micelles using solution NMR spectroscopy.

MATERIALS AND METHODS

Solid-Phase Peptide Synthesis. Drs B2 and [1−23]-Drs B2 were synthesized using solid-phase FastMoc chemistry procedures on an Applied Biosystems 433A automated peptide synthesizer. The sequences of both peptides are shown in Table 1. The peptidyl-resin (Rink amide-MBHA PS resin) and side chain protection bonds were cleaved by incubation in a mixture of 95% trifluoroacetic acid, 2.5% triisopropylsilane, and 2.5% water for 2 h at room temperature (*46*). The resulting mixture was filtered to remove the resin, and the crude peptides were precipitated with cold ether. They were recovered by centrifugation at 5000*g* for 15 min at 4 °C, washed three times with cold ether, dried, dissolved in 10% acetic acid, and lyophilized. The crude peptides were purified by reverse-phase high-performance

Table 1: Amino Acid Sequences, Net Charges, Mean Relative Hydrophobic Moment (μ_H),[a] and Mean Hydrophobicities (H)[a] of Drs B2 and [1−23]-Drs B2

peptide	sequence[b]	charge	μ_H	H
Drs B2	G**L**W**S**K**I**K**E**V**V**GKEAAKAAAKAAGKAA**L**GA**V**SEA**V**$_a$	+3	0.23	−1.97
[1−23]-Drs B2	G**L**W**S**K**I**K**E**V**V**GKEAAKAAAKAAGK$_a$	+4	0.48	−2.76

[a] Mean hydrophobic moment and hydrophobicity were calculated using the CCS scale with the HydroMCalc software (http://www.bbcm.univ.trieste.it/~tossi/HydroCalc/HydroMCalc.html). [b] Highly hydrophobic residues are in bold type; a, amide.

liquid chromatography using a C18 column, and the homogeneity and identity of the peptides were assessed by MALDI-TOF mass spectrometry (Voyager DE PRO, Applied Biosystems) and analytical HPLC.

Antibacterial Assays. Gram-positive eubacteria (*Bacillus megaterium*, *Staphylococcus aureus*, *Staphylococcus hemolyticus*) and Gram-negative eubacteria (*Escherichia coli*, *Pseudomonas aeruginosa*) were cultured, and the minimal inhibitory concentrations (MICs) of peptides were determined as described (*47*). The bacteria were grown in 96-well microtitration plates in the presence of 2-fold serial dilutions of peptide (0−200 μM). Aliquots (10 μL) of each serial dilution were incubated with 90 μL of a suspension of a midlogarithmic phase culture of bacteria at a starting absorbance A_{630} = 0.01 in Poor-Broth nutrient medium (1% bactotryptone, 0.5% NaCl, w/v) (*39*). The inhibition of growth was assessed by measuring the absorbance at 630 nm after 16 h at 37 °C. The minimal inhibitory concentration (MIC) was defined as the lowest concentration of peptide that inhibited the growth of ≥99% of the cells. Bacteria were incubated for 2 h with different concentrations of peptides and plated out on solid culture medium containing 1% noble agar to distinguish between bacteriostatic and bactericidal effects. The plates were subsequently incubated and examined daily for the formation of colonies. All assays were performed in triplicate plus positive controls without peptide and negative controls with 0.7% formaldehyde.

Hemolysis of Rat Red Blood Cells. The hemolytic activity of the peptides was determined using fresh rat erythrocytes. The blood was centrifuged, and the erythrocytes were rinsed three times with PBS (10 mM phosphate buffer, 0.15 M NaCl, 5 mM KCl, pH 7.4). Peptides at different concentrations were incubated with the erythrocyte suspension (10^8 cells/mL in PBS) at 37 °C for 60 min and the erythrocytes removed by centrifugation at 900*g* for 15 min. Hemolysis was assessed by measuring the absorbance at 405 nm of the supernatant. Erythrocytes lysed with 1% (v/v) Triton X-100 were used as a standard for 100% hemolysis.

Cytotoxicity Assay. The Dojindo cell counting kit-8 was used to determine the cytotoxic activity of the peptides. In brief, Chinese hamster ovary (CHO) cells (5000 cells/well) were seeded in 96-well plates 1 day before. The cells were incubated with 10 or 50 μM peptide for 24 h. CCK-8 solution (10 μL) was added to each well. After 3 h incubation, the absorbance was measured at 450 nm; 100% of absorbance was obtained by living cells and adding 0.2% Triton X-100 considered as zero.

Peptide-Induced Permeabilization of the Cytoplasmic Membrane of E. coli. E. coli strain ML-35p was kindly provided by Prof. S. Rebuffat (Muséum National d'Histoire Naturelle, Paris, France). The permeabilization of the cytoplasmic membrane of *E. coli* ML-35p by the peptides was assayed by measuring the β-galactosidase activity with the chromogenic substrate ONPG (*48*). *E. coli* ML-35p, which constitutively expresses β-galactosidase and is lactose permease deficient, was grown in Luria−Bertani broth to stationary phase. Bacteria were washed twice with PBS (10 mM phosphate, 0.15 M NaCl, 0.5 M KCl, pH 7.4) and diluted to an absorbance A_{630} of 0.35 in PBS. Aliquots (15 μL) of the bacterial suspension were then mixed with 2 mM ONPG and incubated with various concentrations of peptides. The hydrolysis of ONPG was monitored every 15 min during 2 h by measuring the absorbance at 405 nm of released *o*-nitrophenol. Complete permeabilization was assessed using 30 μM melittin. All of the results are the means of three to five independent experiments.

Preparation of Multilamellar Vesicles and Large Unilamellar Vesicles. Egg yolk L-α-phosphatidylcholine (PC), egg yolk L-α-phosphatidyl-DL-glycerol (PG), L-α-phosphatidylethanolamine (PE), and calcein were purchased from Sigma. 1-Palmitoyl-2-[1-^{14}C]palmitoylphosphatidylcholine ([^{14}C]PC) was obtained from Amersham. DMPC, DMPE, and DMPG were purchased from Genzyme Pharmaceuticals (Switzerland). PC/PG (3:1 mol/mol), PE/PG (3:1 mol/mol), DMPC, DMPC/DMPG (3:1 mol/mol), and DMPE/DMPG (7:3 mol/mol) multilamellar vesicles (MLV) at the indicated lipid ratios were prepared by dissolving appropriate amounts of phospholipids in chloroform/methanol (1:1 v/v). The samples were then dried under a nitrogen stream, and films were kept under vacuum for 3 h to remove all traces of organic solvents. The resulting lipid films were warmed together with PBS buffer (10 mM phosphate, 100 mM NaCl, pH 7.3) in a thermostated water bath at ca. 10 °C above the temperature of the gel-to-liquid crystalline phase transition (T_m), hydrated at the same temperature, and then vortexed to obtain MLVs. The multilamellar vesicles were frozen in liquid nitrogen and thawed in a water bath at ca. 10 °C above T_m, and this process was repeated seven times. PC/PG (3:1 mol/mol), PE/PG (3:1 mol:mol), DMPC, DMPC/DMPG (3:1 mol/mol), and DMPE/DMPG (7:3 mol/mol) large unilamellar vesicles (LUV) at the indicated lipid ratios were obtained from the MLVs by extrusion as described in ref *49*. The calcein-containing LUVs, containing [^{14}C]PC at a 0.01 molar ratio and 70 mM calcein in 10 mM HEPES, pH 7.4, were prepared as described in ref *50*. The final lipid concentration was quantified, measuring the [^{14}C]PC radioactivity with a liquid scintillation counter LS 6000 SC (Beckman Coulter, France).

Peptide Binding to LUVs. Peptide binding to membranes was measured by following the change in the fluorescence emission peak of tryptophan as described in ref *50*. The excitation wavelength was 280 nm, and the emission spectrum was collected (290−600 nm). A cross-oriented configuration of the polarizer (ex_{pol} = 90°, em_{pol} = 0°) was used in order to reduce LUV diffusion artifacts.

Measurement of Calcein Leakage from LUVs. The release of calcein after 5 min of peptide exposure to LUVs was measured as described in ref *50*. The spontaneous leakage of calcein in the absence of peptide was found to be

negligible. Leakage was expressed as a percent relative of the total amount of dye released by LUVs after lysis with 1% Triton X-100 according to the equation % release = $100(F(t) - F_0)/(F_T - F_0)$. $F(t)$ is the fluorescence intensity at time t, F_0 is the fluorescence intensity before peptide addition, and F_T is the fluorescence intensity after LUV lysis.

Differential Scanning Calorimetry. Experiments were performed using a Nano-DSC III calorimeter (Calorimetry Sciences Corp., Provo, UT) as described in ref *51*. Buffers and MLVs were degassed under vacuum for 20 min prior to being loaded into the machine. Samples were loaded below the main phase transition temperature for the lipid mixture and put under 3.0 atm of pressure. Ten scans were run for each sample, with 10 min equilibration time between each scan. Heating and cooling rates of 0.5 and 1 °C/min, respectively, were used over a temperature range of 0−40 °C for DMPC and DMPC/DMPG (3:1 mol/mol) and 10−60 °C for DMPE/DMPG (7:3 mol/mol). The raw data corresponding to the heating scans were converted to molar heat capacity, and the values for transition temperature and enthalpy were estimated using CpCalc software. For each conversion, the average lipid molecular weight for each sample and a partial specific volume of 0.730 mL/g were used.

Circular Dichroism. CD measurements were performed in a Jobin Yvon CD6 dichrograph linked to a PC microprocessor (*52*). Measurements were performed with 1 mg/mL liposomes at 25 °C by using a quartz cuvette (Hellma) with a path length of 0.1 cm. All of the measurements were performed with peptide/lipid molar ratios ranging from 1:100 to 1:20 in 10 mM phosphate buffer (pH 7.4), and peptides were added to the lipid suspensions immediately before measurement. Experimental conditions were as follows: 2 nm bandwidth, 0.5 nm resolution, and 1 s time response. In most cases, each spectrum was the average of five accumulations. Spectra of pure liposomes were run as blank to be subtracted from the liposome/peptide spectra. Circular dichroism measurements are reported as $\Delta\epsilon/n$, where $\Delta\epsilon$ is the dichroic increment ($M^{-1}\cdot cm^{-1}$) and n is the number of residues in the peptide. The relative helix content was estimated according to the relation % helix = $-[\Delta\epsilon_{222nm} \times 10]/n$, where $\Delta\epsilon_{222nm}$ is the dichroic increment at 222 nm.

NMR Spectroscopy. The NMR samples were prepared in 550 μL of H_2O/D_2O (90:10 v/v) or D_2O in the presence of 80 mM SDS-d_{25} (Eurisotop, France) and using peptide concentrations from 25 μM to 1.4 mM. The pH was set to 5.5 using microliter amounts of NaOH. Sodium 3-(trimethylsilyl)propionate-2,2,3,3-d_4 (Isotec; Sigma Aldrich) was used as an internal reference (0.1 mM) for chemical shift calibration. The NMR experiments were recorded on a Bruker Avance III spectrometer equipped with a $^1H/^{13}C/^{15}N/^2H$ Z-gradient TCI cryoprobe and operating at a ^1H frequency of 500 MHz. Spectra were recorded at a temperature of 309.5 K. Two-dimensional homonuclear TOCSY, DQF-COSY, and NOESY experiments were collected with 512 t_1 increments and 4096 data points in t_2 over a spectral width of 12 ppm in both dimensions. A DIPSI-2 mixing scheme (*53*) was used in the TOCSY experiments with durations of 22−70 ms. NOESY experiments were recorded with mixing times of 50 and 200 ms. The solvent signal was suppressed by a WATERGATE sequence (*54*) and water flip-back pulses (*55, 56*). A natural abundance 2D $^1H-^{15}N$ HSQC spectrum was recorded using a WATERGATE sequence and water flip-back pulses (*57*). 2D $^1H-^{13}C$ HSQC spectra were recorded using gradient pulses for coherence selection (*58*). The exchange kinetics of the amide proton was monitored on 1D spectra after resuspending in D_2O a lyophilized peptide sample. NMR experiments were processed with the Bruker TOPSPIN program. Time−domain data were typically multiplied by shifted sine-bell functions and zero-filled prior to Fourier transformation. Indirect dimensions were extended by linear prediction. Baseline distortions were corrected with a fifth order polynomial function. Spectra were analyzed with the aid of the XEASY program (*59*). The chemical shift deviations (CSDs) of ^1H and ^{13}C resonances were calculated using a set of random coil values reported in water (*60*). $^3J_{HN-H\alpha}$ coupling constants were measured with the INFIT program from F_2 rows selected on a 2D TOCSY spectrum (*61*).

NMR Restraints. Interproton distance restraints were estimated from NOESY cross-peak intensities. Three upper limit classes of 3.0, 3.8, and 5.0 Å were defined depending on cross-peak intensities in the NOESY spectra. The TALOS program (*62*) was used to derive backbone dihedral angle restraints using ^{15}N, $^{13}C^{\alpha}$, $^{13}C^{\beta}$, and $^1H^{\alpha}$ chemical shifts. The ϕ, ψ torsion angles of residues that were consistently predicted to fall into the α_R region of the Ramachandran map were restrained around $-60° \pm 30°$ and $-40° \pm 30°$, respectively.

Structure Calculation. A set of 50 structures was calculated by torsion angle dynamics in DYANA using standard parameters (*63*). The best 25 structures having the lowest target function were then minimized using the XPLOR-NIH program (*64*) and CHARMM22 force field. Nonbond terms consisted of a Lennard-Jones potential and an electrostatic potential with a distance-dependent dielectric $\epsilon = 4r$. The 20 structures exhibiting the lowest energies were selected to represent the NMR ensemble. Structures were analyzed using InsightII (Accelrys, San Diego, CA) and PROCHECK-NMR programs (*65*).

RESULTS

Antibacterial Activities of Drs B2 and [1−23]-Drs B2. Drs B2 and [1−23]-Drs B2 were tested for their antibacterial activity against five strains of bacteria including the three Gram-positive bacteria *B. megaterium* (soil bacterium), *S. aureus*, and *S. hemolyticus* (opportunistic human pathogens) and the two Gram-negative bacteria *E. coli* and *P. aeruginosa* (opportunistic human pathogens). As shown in Table 2, Drs B2 inhibited the growth of all strains, with minimal inhibitory concentrations in the low micromolar range. The dose−response profiles showed sharp curves in which 0−100% inhibition was generated within a 1−2-fold peptide dilution (not shown). When MIC well contents were spread on agar plates and incubated overnight at 37 °C, no bacterial growth was observed, indicating that Drs B2 is bactericidal. Whereas Drs B2 was active against all of the tested bacteria, [1−23]-Drs B2 was virtually inactive or poorly active against all of the tested bacteria but active against *B. megaterium.*

Permeabilization of the Bacterial Cytoplasmic Membrane. The disruption of the bacterial membrane by Drs B2 and [1−23]-Drs B2 was detected by measuring the hydrolysis of the chromogenic substrate, ONPG, by the cytoplasmic

Table 2: Antimicrobial, Hemolytic, and Cytotoxic Activities of Drs B2 and [1−23]-Drs B2

	Drs B2	[1−23]-Drs B2
	minimal inhibitory concn (μM)[a]	
Gram-negative bacteria		
P. aeruginosa	3.1	100
E. coli B	0.8	50
Gram-positive bacteria		
S. hemolyticus	12.5	R[b]
S. aureus	0.7	25
B. megaterium	0.3	1.5
	% hemolysis at 50 μM[c]	
erythrocytes	0	0
	% cytotoxicity at 10 μM (50 μM)[c]	
CHO cells	0 (50)	0 (0)

[a] The antimicrobial activity is expressed as MIC (μM), the minimal peptide concentration required for total inhibition of cell growth in liquid medium. [b] Strains were considered resistant (R) when their growth was not inhibited by peptide concentrations up to 200 μM. [c] See Materials and Methods section.

β-galactosidase of the permease-deficient strain *E. coli* ML-35p after incubation with the peptides (0−50 μM). Drs B2 was as efficient as melittin to permeabilize the cytoplasmic membrane, as shown by the increase in release of enzyme with increasing concentrations of peptide, and ~100% enzyme activity was released after 120 min of incubation even at the lowest peptide concentration shown to cause bacterial death (Figure 1). These data confirm that the bacterial membrane is one of the main targets of Drs B2. In contrast, [1−23]-Drs B2 was found to be poorly efficient in permeating the bacterial membrane even at high peptide concentrations (Figure 1).

Cytotoxic and Hemolytic Activities. Tests of the peptides' hemolytic activity against rat erythrocytes (Table 2) showed that Drs B2 and [1−23]-Drs B2 have no hemolytic activity above the MIC values observed for most of the bacterial strains tested. The cytotoxic activities of Drs B2 and [1−23]-Drs B2 against mammalian cells were evaluated on CHO cells by using 2-(2-methoxy-4-nitrophenyl)-3-(4-nitrophenyl)-5-(2,4-disulfophenyl)-2*H*-tetrazolium that gives a water-soluble, yellow-colored formazan dye upon reduction by dehydrogenases in living cells. As shown in Table 2, Drs B2 and [1−23]-Drs B2 were not toxic at 10 μM. However, 50% of CHO cells were found to be killed by 50 μM Drs B2 after 24 h, whereas no cytotoxic activity was found for [1−23]-Drs B2 at the same concentration.

Phospholipid Vesicle-Disrupting and Vesicle-Binding Activities of Drs B2 and [1−23]-Drs B2. The outer leaflet of the cytoplasmic membrane of Gram-positive and Gram-negative bacteria is rich in anionic phospholipids, such as phosphatidylglycerol (PG) and cardiolipin (CL), e.g., *S. aureus* (58% PG, 42% CL). It may also contain high amounts of zwitterionic phosphatidylethanolamine (PE), e.g., *E. coli* (80% PE, 15% PG) and *B. megaterium* (70% PE, 30% PG plus CL). The zwitterionic phospholipids phosphatidylcholine (PC) and PE are the major lipid components in animal cell membranes, but PC is mainly found in the outer leaflet, whereas PE is mainly found in the inner leaflet of the bilayer. Therefore, the membrane-disrupting activities of Drs B2 and [1−23]-Drs B2 were investigated by calcein release from negatively charged PE/PG (3:1 mol/mol) and PC/PG (3:1 mol/mol) LUVs as model systems for bacterial membranes. The idea behind the use of these two binary lipid mixtures

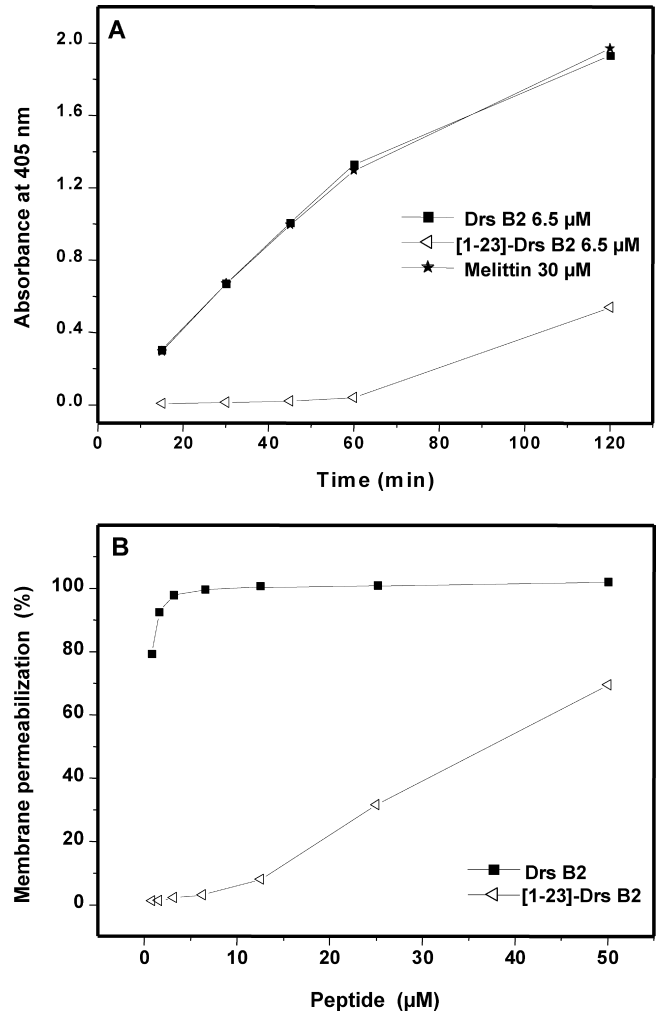

FIGURE 1: Bacterial membrane permeabilization by Drs B2, [1−23]-Drs B2, and melittin. (A) Kinetics of the cytoplasmic membrane leakage of *E. coli* ML-35p after treatment with 6.5 μM Drs B2 or [1−23]-Drs B2 or 30 μM melittin. The membrane leakage was followed by measuring the hydrolysis of ONPG at 405 nm by the cytoplasmic bacterial β-galactosidase in the filtrate of the *E. coli* culture after incubation with the peptides (see Materials and Methods). (B) Membrane permeabilization of *E. coli* ML-35p observed after treatment for 1 h with increasing concentrations of Drs B2 or [1−23]-Drs B2.

was to examine the effect of the nature of the zwitterionic lipid component on the binding/disrupting efficiencies of the peptides while keeping a constant net charge of the anionic bilayer. Figure 2A displays the calcein leakage as a function of peptide concentration. As observed by the peptide/lipid ratio for half-maximal calcein release ($P/L_{50\%}$), Drs B2 had much more effective membrane-disrupting activity against PE/PG LUVs ($P/L_{50\%}$ 1/150) as compared to that of [1−23]-Drs B2 ($P/L_{50\%}$ 1/30). However, both peptides were effective at inducing leakage in PC/PG lipid vesicles.

The ability of the peptides to bind to PE/PG and PC/PG LUVs was monitored by fluorescence spectroscopy by following the extent of Trp fluorescence blue shift at 295 nm. As shown in Figure 2B, both peptides showed comparable blue shifts in the presence of PE/PG or PC/PG LUVs, consistent with a membrane interaction. Moreover, both peptides attained binding saturation at a similar peptide/lipid molar ratio (about 1/40) in both types of vesicles. This showed that differences in the peptide leakage efficiencies did not result from different amounts of bound peptides and

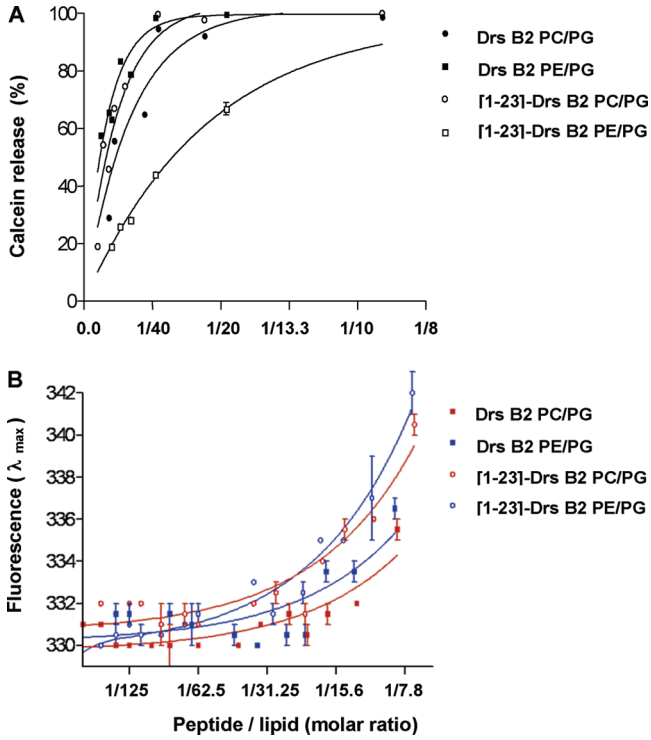

FIGURE 2: Phospholipid vesicle-disrupting and vesicle-binding activities of Drs B2 and [1−23]-Drs B2. (A) Permeabilization measured by calcein release of PE/PG (3:1 mol/mol) and PC/PG (3:1 mol/mol) large unilamellar vesicles by Drs B2 and [1−23]-Drs B2 as a function of peptide/lipid ratio (P/L). (B) Binding of DrS B2 and [1−23]-Drs B2 to PE/PG (3:1 mol/mol) and PC/PG (3:1 mol/mol) large unilamellar vesicles. Peptide binding was followed by the change in the emission fluorescence peak from 343 nm in aqueous solution to 330 nm for bound peptides.

that [1−23]-Drs B2 attain the $P/L_{50\%}$ of lysis only close to binding saturation.

Comparing the Interaction of Drs B2 and [1−23]-Drs B2 with Zwitterionic and Anionic Model Membranes by Differential Scanning Calorimetry. Differential scanning calorimetry was used to study the thermotropic behavior of multilamellar vesicles upon addition of Drs B2 and [1−23]-Drs B2. DMPC, a zwitterionic phospholipid, was used as a model for mammalian cell membranes. DMPC/DMPG (3:1 mol/mol) and DMPE/DMPG (7:3 mol/mol) were chosen as a model system for bacterial membranes. In the absence of peptide, DMPC MLVs exhibit two endothermic events on heating, i.e., a weakly energetic pretransition near 13 °C (conversion of the ordered lamellar gel phase, $L\beta'$, with tilted hydrocarbon chains to the ordered rippled gel phase $P\beta'$) and a strongly energetic and highly cooperative main transition near 24 °C (conversion of the rippled gel phase to the fluid lamellar liquid-crystalline phase Lα) (Figure 3A) (*66*). The pretransition is due to interactions between the head groups of the phospholipids, and increasing the distance between them causes the pretransition peak to disappear. Because the pretransition is exquisitely sensitive to the presence of a small amount of exogenously added substances, it is not a good indicator of either strong disturbance in the membrane or deep peptide penetration in the bilayer (*67*). The main phase transition (chain melting) is mainly due to *trans*−*gauche* interconversion of the acyl chains, which decreases the acyl chain packing of the lipid molecules, increasing fluidity of the membrane. Therefore, the effect of added peptides on the temperature (T_m), enthalpy (ΔH), and cooperativity ($\Delta T_{1/2}$) of the main transition serves as an indicator of the ability of the peptide to interact with lipid head groups and to perturb the packing of the lipid acyl chains (*68*−*70*). The addition of Drs B2 to zwitterionic DMPC vesicles leads to a significant decrease (∼52%) in the enthalpy of the main transition (Figure 3A, Table 3). The enthalpy of the main transition is mainly due to the disruption of intra- and intermolecular van der Waals interactions that lead to chain melting, indicating some level of peptide insertion within the acyl chain region. However, no significant effect on the temperature and cooperativity of the main phase transition was observed, indicating that Drs B2 interacts with the polar head groups and glycerol backbone region of the phospholipids only. Regarding [1−23]-Drs B2 interaction with DMPC MLVs, no major effects were observed for the main phase transition. The T_m, half-width, and shape of the peak change little from those of pure DMPC throughout the peptide concentration range, and only a small change (∼20%) in the enthalpy was observed. These results are consistent with a weak interaction of [1−23]-Drs B2 with DMPC.

Drs B2 exhibited strong perturbing effects on the phase behavior of negatively charged MLVs. In the absence of peptide, DMPC/DMPG MLVs exhibit a weakly energetic pretransition near 13 °C and a more energetic phase transition near 24 °C. The addition of Drs B2 strongly reduces the enthalpy of the transition (∼48%), together with broadening of the peak, indicating some level of peptide insertion within the acyl chain region and the apparition of a shoulder at the right wing of the main phase transition thermogram (Figure 3B). Increasing quantities of the peptide induced a two-component main phase transition consisting of a broad, higher temperature and less cooperative component superimposed over a sharper, lower temperature component. (Figure 3B). Using the rationale provided by previous studies (*71*), the sharp and broad components of the DSC endotherms were assigned to the chain melting phase transition of peptide-poor and peptide-rich phospholipid domains, respectively. As for Drs B2, the presence of increasing quantities of [1−23]-Drs B2 results in reduced cooperativity of the main transition and the induction of a two-component main phase transition, with a more cooperative lower temperature endotherm superimposed over a less cooperative higher temperature endotherm (Figure 3B). However, the enthalpy of the transition changes little from that of pure DMPC/DMPG throughout the peptide concentration range (Table 3), suggesting that [1−23]-Drs B2 resides in the lipid head group region and does not penetrate deeply into the hydrophobic part of the bilayer.

On the other hand, Drs B2 caused a very different perturbing effect than [1−23]-Drs B2 on the thermotropic phase behavior of DMPE/DMPG MLVs. As can be seen in panel C of Figure 3, the lipid mixture produced a single, although broad transition confirming good lipid miscibility. The electrostatic and H-bond interaction networks at the surface of a PE bilayer are quite strong and are responsible for the high transition temperature of this lipid. Consequently, these networks are more likely to favor PE−PE interactions over PE−peptide interactions unless the peptide significantly disrupts the cohesion of the bilayer. As shown in Figure 3C and Table 3, Drs B2 produced a significant decrease in the

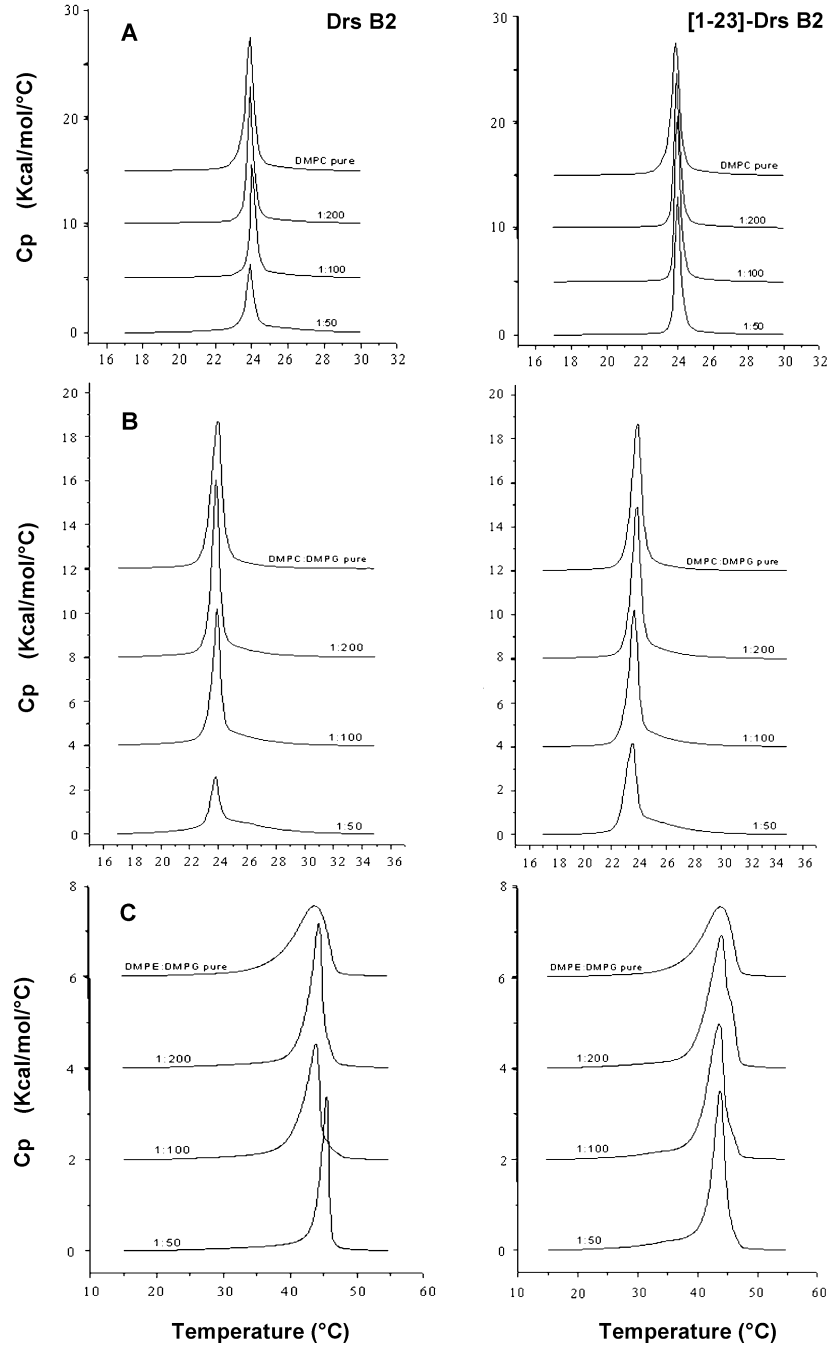

FIGURE 3: High-sensitivity DSC heating scans illustrating the effect of Drs B2 (left panel) and [1−23]-Drs B2 (right panel) on the thermotropic phase behavior of zwitterionic and anionic multilamellar phospholipid vesicles. (A) DMPC MLVs. (B) DMPC/DMPG (3:1 mol/mol) MLVs. (C) DMPE/DMPG (7:3 mol/mol) MLVs. Scans were acquired at different peptide/lipid molar ratios (1/200, 1/100, 1/50).

enthalpy of the transition (∼30%), indicating that the peptide perturbs the acyl chain packing through interactions with the polar head groups and glycerol backbone region of the phospholipids and the region of the lipid acyl chain near the bilayer surface. In addition, with the increase in the P/L ratio, the lipid phase transition occurs at higher temperatures and becomes less broad until it collapses into a single sharp transition located around 45.5 °C, suggesting lipid demixing. In contrast, [1−23]-Drs B2 produced a significant increase in the enthalpy of the transition without effect in the lipid phase transition temperature, indicating that the peptide interacts "atmospherically" at the head group level without penetrating and perturbing the hydrophobic core of the vesicles (Figure 3C, Table 3).

Effects of Drs B2 and [1−23]-Drs B2 on the Lipid Membrane Curvature. The effect of Drs B2 and [1−23]-Drs B2 on the membrane monolayer curvature strain was determined by the shift in the lamellar (Lα) to hexagonal (H_{II}) phase transition temperature (T_H) of DiPoPE. The shift in T_H is a consequence of the stability of the phase and changes in monolayer curvature (*72*). As shown in Figure 4 and Table 3, the lipid alone exhibited a T_H of 41.5 °C. Both peptides led to a similar increase in T_H to 46.8−48 °C, indicating that they induce a positive curvature strain in the lipid bilayers. However, only Drs B2 produced a marked decrease in the enthalpy of the transition, suggesting that it perturbs the lipid phase transition by interacting with the fatty acyl chains.

Table 3: Thermotropic Behavior of DMPC, DMPC/DMPG (3:1 mol/mol), DMPE/DMPG (7:3 mol/mol), and DiPOPE Multilamellar Vesicles upon Addition of Drs B2 or [1−23]-Drs B2[a]

		Drs B2		[1−23]-Drs B2	
MLV	P:L ratio	T_m (°C)	ΔH (kcal·mol^{-1})	T_m (°C)	ΔH (kcal·mol^{-1})
DMPC	0	23.9	7.9	23.9	7.9
	1:200	23.9	5.9	24	7.0
	1:100	24	4.9	24	6.9
	1:50	23.9	3.8	24	6.3
DMPC/DMPG	0	23.9	7.0	23.9	7.0
	1:200	23.8	6.8	23.9	6.9
	1:100	23.9	5.7	23.7	6.9
	1:50	23.8	3.7	23.6	6.3
DMPE/DMPG	0	43.8	9.3	43.8	9.3
	1:200	44.3	9.2	44.0	13.4
	1:100	43.9	8.9	43.8	12.4
	1:50	45.5	6.6	43.8	11.7
DiPOPE	0	41.5	0.2	41.5	0.2
	1:50	46.8	0.05	48.0	0.2

[a] Phase transition temperature (T_m) and total enthalpy for gel-to-liquid crystalline transition of MLVs with and without Drs B2 or [1−23]-Drs B2 are indicated. Phase transition temperature and total enthalpy were estimated by a peak-fitting procedure using CPCalc software.

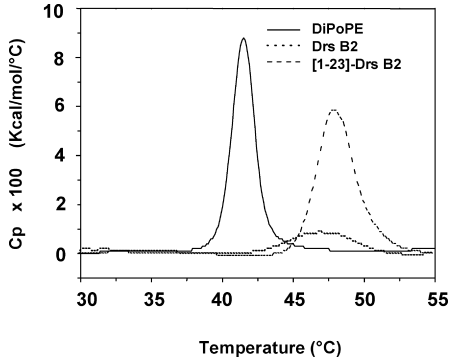

FIGURE 4: High-sensitivity DSC heating scans illustrating the effect of Drs B2 and [1−23]-Drs B2 on the thermotropic phase behavior of DiPoPE multilamellar phospholipid vesicles. The lamellar (Lα) to hexagonal (H_{II}) phase transition temperature (T_H) observed is 41.5, 46.8, and 48 °C for the lipid alone and in the presence of Drs B2 and [1−23]-Drs B2, respectively.

Secondary Structure of Membrane-Bound Drs B2 and [1−23]-Drs B2 Inferred from CD Spectroscopy. Preliminary indications of the peptides' secondary structure when bound to different phospholipid vesicles were obtained by CD measurements in water and in the presence of DMPC, DMPC/DMPG (3:1 mol/mol), and DMPE/DMPG (7:3 mol/mol) LUVs (Figure 5). All experiments were performed at P/L ratios ranging from 1/200 to 1/20 in sodium phosphate buffer, pH 7.4. The CD spectra of the peptides in aqueous solution have a single negative band at 198 nm, typical of peptides in random coil conformation (not shown). Drs B2 adopts an α-helix conformation with the characteristic minima at 208 and 222 nm and had similar helix contents (52−68% α-helix) when mixed with anionic vesicles or zwitterionic vesicles. Thus, once the peptide is bound to a zwitterionic lipid bilayer, it adopts the same secondary structure as with a negatively charged bilayer. Like Drs B2, [1−23]-Drs B2 had helical ordered structures (38−54% α-helix) when mixed with anionic vesicles but exhibited very little ordered structure when mixed with zwitterionic lipids (Figure 5). Partitioning of cationic Drs B2 and [1−23]-Drs B2 into zwitterionic DMPC vesicles can be accounted for mainly by their hydrophobicity, stressing the importance of hydrophobic interactions between the peptides and the lipid bilayer for helix formation and stabilization (*73*).

Comparing the Membrane-Bound Three-Dimensional Structures of Drs B2 and [1−23]-Drs B2 by NMR Spectroscopy in Micellar SDS. The structure of the truncated [1−23]-Drs B2 analogue in SDS micelles was analyzed by NMR spectroscopy combined with molecular dynamics calculations. The conformational properties of the truncated analogue were compared with full-length Drs B2 whose structure was previously reported in SDS (*42*). NMR spectra were recorded in 80 mM SDS in water. Since Drs B2 was previously found to exhibit complex slow-exchange equilibrium at high peptide concentration (*42*), the NMR study was carried out with peptide concentrations ranging from 20 μM to 1.4 mM, the SDS micelle concentration being kept constant (∼1.4 mM, assuming a number of 60 SDS molecules per micelle). 1D ^{1}H spectra recorded with [1−23]-Drs B2 concentrations between 20 μM and 0.12 mM did not show significant chemical shift variations of proton resonances. The comparison of 1D and 2D TOCSY spectra recorded with peptide concentrations of 0.12 and 1.4 mM showed modifications of HN and Hα resonances: a slight broadening of several resonances was observed together with small chemical shift variations (<0.02 ppm). Furthermore, several residues exhibited a second set of chemical shifts, their values remaining very close to the former one (<0.03 ppm for HN resonances). Altogether, these observations suggest that, in the presence of SDS micelles, oligomerization of [1−23]-Drs B2 occurs in the millimolar range. Note, however, that millimolar concentrations are well above the highest MIC of the peptide (Table 2). Since the proton chemical shifts remain very similar, the overall conformation of the peptide does not seem to be altered by the oligomerization equilibrium. Consequently, the complete NMR structural study was performed at the highest concentration tested (1.4 mM).

Complete sequence-specific resonance assignments of [1−23]-DrsB2 were obtained from the analysis of through-bond scalar connectivities in 2D TOCSY and 2D DQF-COSY spectra, together with though-space dipolar connectivities in 2D NOESY spectra. Natural-abundance ^{13}C−^{1}H and ^{15}N−^{1}H 2D HSQC were also recorded to facilitate assignments and provide additional conformational parameters. Surprisingly, the truncated [1−23]-Drs B2 analogue shows significant chemical shift differences with full-length Drs B2 (studied in 80 mM SDS at a concentration of 0.5 mM). The chemical shift deviations (CSDs) of the H^α resonances of the two peptides are shown in Figure 6 for comparison. The H^α CSDs, which correspond to the differences between observed chemical shifts and corresponding random coil values, are good indicators of the local backbone conformations of each residue (*60*). On the whole the two peptides show large upfield shifts of H^α resonances (corresponding to negative CSDs), reflecting the high helical propensity of most residues. The CSDs are weaker for the last residues of [1−23]-Drs B2 (21−23), which can be ascribed to the peptide sequence shortening on the C-terminal side. Unexpectedly, major differences are observed between the two peptides for the central Val^9 and Gly^{10} residues. These residues have zero or positive CSD values in Drs B2 whereas uninterrupted negative CSD values are observed in

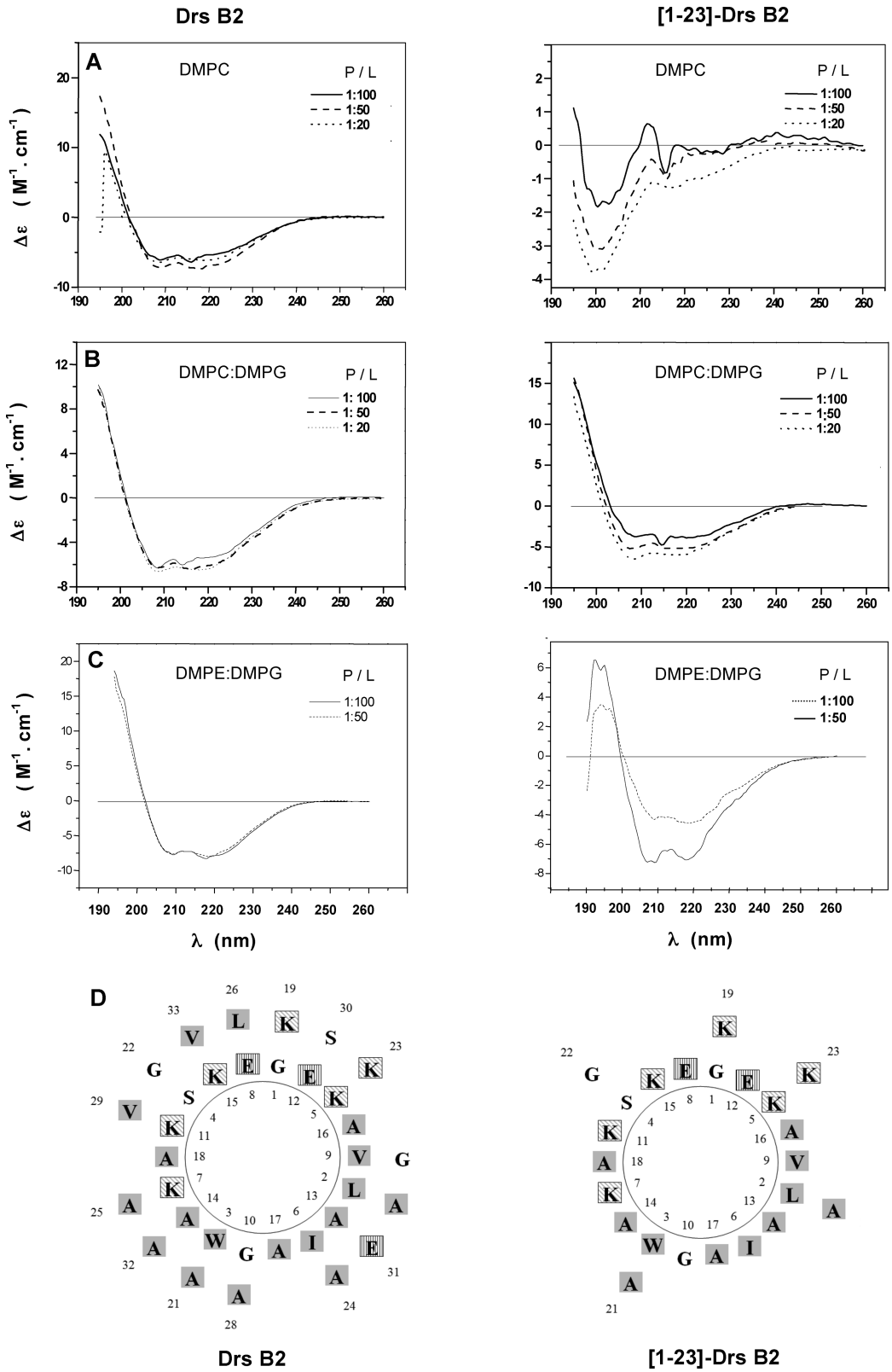

FIGURE 5: Secondary structure of membrane-bound Drs B2 (left panel) and [1−23]-Drs B2 (right panel) to zwitterionic and anionic large unilamellar vesicles. CD spectra of the peptides in the presence of (A) DMPC LUVs, (B) DMPC/DMPG (3:1 mol/mol) LUVs, and (C) DMPE/DMPG (7:3 mol/mol) LUVs. Peptides were added to the lipid suspensions immediately before measurement. (D) Helical wheel projections of the peptides. The amphipathic nature of the α-helical projections is highlighted with the hydrophobic residues shaded and the charged residues hatched.

the corresponding segment of [1−23]-Drs B2. A large difference is also observed in the N-terminal region concerning the Leu[2] residue. The conformation of [1−23]-Drs B2 was further examined by analyzing chemical shift data, $^{3}J_{HN-H\alpha}$ coupling constants, and interproton NOEs (Figure 7). The analysis of $^{1}H^{\alpha}$, $^{13}C^{\alpha}$, $^{13}C^{\beta}$, and ^{15}N chemical shifts with the TALOS program indicated that most residues adopt α_R conformations, confirming the H^{α} CSD analysis (Figure 7). NOE correlations characteristic of α-helical conformation are observed (Figure 7), namely, strong $d_{NN}(i,i+1)$ and

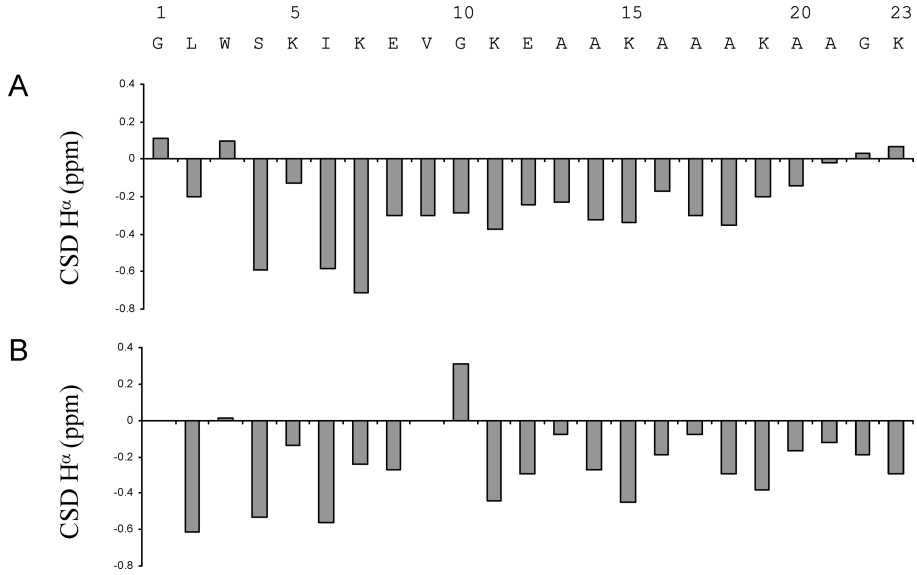

FIGURE 6: Chemical shift deviation (CSD) of H^{α} resonances of [1−23]-DrsB2 (A) and Drs B2 (B) peptides in 80 mM SDS. Residues 24−33 of Drs B2 are not shown. The CSD values were calculated as the differences between observed chemical shifts and random coil chemical shifts.

FIGURE 7: Summary of NMR conformational parameters of [1−23]-Drs B2 in SDS. The α symbol indicates residues that were consistently predicted by the TALOS program to fall into the α_R region based on chemical shift data. $^3J_{HN-H\alpha}$ coupling constants are represented by circles: open circle, $J < 6$ Hz; gray circle, $6 \leq J < 8$ Hz; filled circle, $J \geq 8$ Hz. The side chain χ^1 rotamers that could be determined from NOE analysis are indicated: t, *trans* ($\chi^1 \sim 180°$); g^-, *gauche*$^-$ ($\chi^1 \sim -60°$). The relative intensity of NOE connectivities is indicated by horizontal bars of varying thickness.

medium $d_{\alpha N}(i,i+1)$ sequential NOEs, together with medium-range $d_{\alpha N}(i,i+3)$, $d_{\alpha N}(i,i+4)$, and $d_{\alpha\beta}(i,i+3)$ NOEs. Most non-glycine residues are characterized by small values of $^3J_{HN-H\alpha}$ coupling constants that are compatible with ϕ angles around −60° typically observed in helical conformations (Figure 7). The larger value of the Val^9 $^3J_{HN-H\alpha}$ coupling constant (6.5 Hz) may correspond to a more negative ϕ angle value (∼−80°), other NMR parameters indicating that this residue preferentially adopts an α_R conformation.

The NMR structures of [1−23]-Drs B2 were calculated by restrained molecular dynamics in DYANA and refined by energy minimization with XPLOR-NIH and CHARMM22 force field. The final structures have good geometrical quality and show few restraint violations. The rmsd calculated on backbone atom positions is 1.98 Å. A well-defined amphipathic α-helical conformation extends over residues 2−20 (Figure 8), with a backbone rmsd of 0.58 Å. The central Gly^{10} residue does not induce disruption of the α-helix. Trp^3, Ile^6, and Val^9 side chains are well-defined and adopt a unique conformation around their χ^1 angle, as determined by the NOE analysis. The N-terminal part is stabilized by many van der Waals contacts between Leu^2, Trp^3, Ile^6, and Val^9 side chains. A π-cation interaction is also observed between Trp^3 and Lys^7 side chains, as evidenced by NOEs, upfield shifts, and large chemical shift difference between CH_2^{ϵ} protons of Lys^7. All of these interactions define a large hydrophobic core in the N-terminal region. The amide protons of Ile^6 and Lys^7 have the slowest exchange rates, indicating that they are involved in stable hydrogen bonds and are not solvent-exposed. Electrostatic interactions between Glu and Lys side chains are observed in some calculated structures, involving Lys^5/Glu^8, Lys^{11}/Glu^8, and Lys^{15}/Glu^{12} pairs.

DISCUSSION

Shortening the peptide chain of Drs B2 to [1−23]-Drs B2 greatly alters the biological activities of the peptide, impairs its capacity to perturb and disrupt phospholipid bilayers, and also affects its membrane-bound three-dimensional structure. First, Drs B2 exhibited strong antimicrobial activities against Gram-positive and Gram-negative bacteria at micromolar or submicromolar concentrations in contrast to the truncated analogue that showed considerably reduced efficacy and restricted spectrum of activity. Second, Drs B2 was highly effective at permeabilizing the cytoplasmic membrane of *E. coli* at concentrations comparable to MIC values as shown by unmasking of cytoplasmic β-galactosidase activity to a nonpermeant substrate. [1−23]-Drs B2 was much less effective than Drs B2 to permeabilize the membrane of *E. coli* in vivo even at high peptide concentrations. Third, calorimetric studies indicated that Drs B2 induced a strong perturbation in the lipid chain packing of anionic MLV mimicking prokaryotic membranes through preferential electrostatic interactions with the polar head groups and glycerol backbone region of the anionic phospholipids and

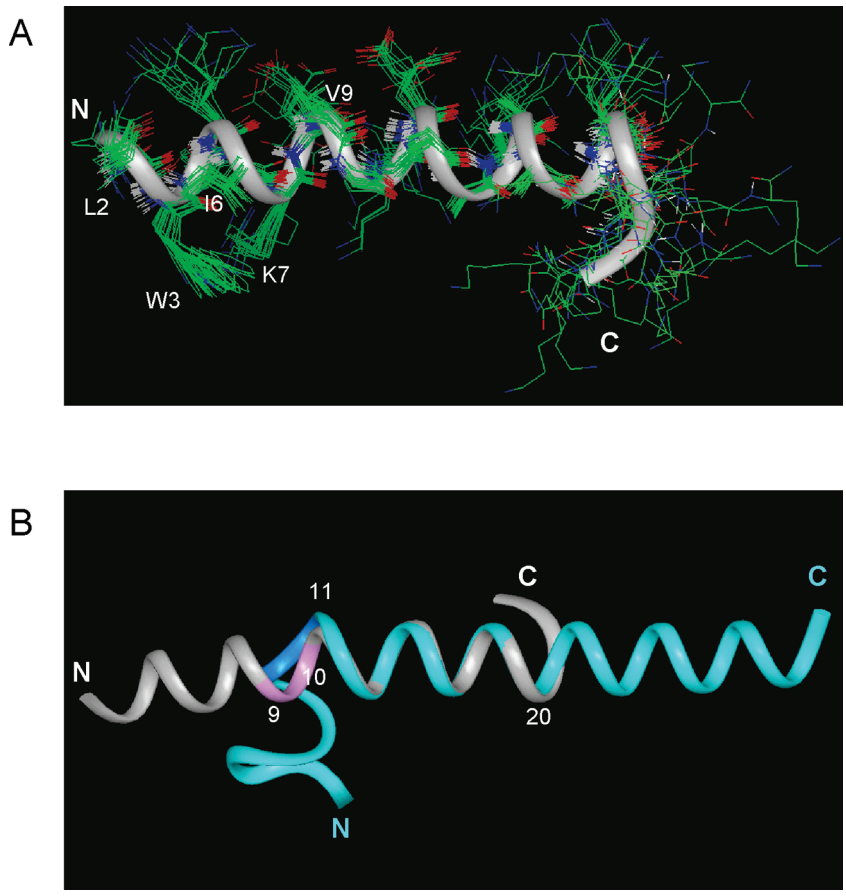

FIGURE 8: NMR structures of [1−23]-DrsB2 and Drs B2 in SDS. (A) Family of 20 structures obtained from NMR data for [1−23]-Drs B2. Structures were superimposed by best fitting of backbone N, C^{α}, and C′ atoms of residues 2−20 to the lowest energy structure. The backbone of the lowest energy structure is shown as a ribbon. Atoms are shown with different colors (amide hydrogen, white; carbon, green; nitrogen, blue; oxygen, red). (B) Comparison of the backbone conformations of [1−23]-Drs B2 (gray) and Drs B2 (cyan) (*14*). Structures were superimposed by fitting to segment 11−20. The Val^{9}-Gly^{10} segment is enlightened in each structure. N and C: N- and C-terminus.

hydrophobic interactions with the lipid acyl chain near the bilayer surface. In contrast, [1−23]-Drs B2 interacts "atmospherically" at the head group level through electrostatic interactions without penetrating and perturbing the hydrophobic core of the vesicles. Finally, the truncation of the C-terminal part of Drs B2 had marked effects on the conformational properties of the peptide when bound to phospholipid vesicles or to SDS anionic micelles. Whereas Drs B2 is structured in the α-helix when mixed with anionic vesicles or zwitterionic vesicles, [1−23]-Drs B2 exhibits an α-helical conformation only when mixed with anionic vesicles. Moreover, DrsB2 and [1−23]-Drs B2 adopted different structures in the presence of SDS micelles. Drs B2 was found to adopt a well-defined amphipathic helix spanning residues 11−31, connected by a hinge region (Val^{9}-Gly^{10}) to a loosely defined helical N-terminal segment. In contrast, [1−23]-Drs B2 adopts a well-defined helix encompassing residues 2−20, which is not interrupted around the Val^{9}-Gly^{10} pair.

Detailed analyses of these results provide important information on the mechanism of action of Drs B2. Although Drs B2 and [1−23]-Drs B2 strongly bind to anionic vesicles, calcein-leakage assays showed that Drs B2 is much more effective than the truncated analogue at inducing leakage in PE/PG vesicles mimicking the bacterial membrane. However, both peptides induced leakage of PC/PG vesicles with similar potencies. This observation can be rationalized on the basis of the strong electrostatic and H-bonding rigid networks between the polar head groups at the surface of PE/PG bilayers favoring the gel over fluid liquid-crystalline phases (*74, 75*). With PC/PG bilayers, there are no H-bonding donor groups on the polar head groups, and electrostatic repulsion between phosphate moieties at the surfaces prevails, favoring the fluid liquid-crystalline over gel phases. Consequently, PE/PG bilayers are much more difficult to disrupt than PC/PG bilayers unless the peptide, such as Drs B2, significantly affects the cohesion of the hydrophobic core of the membrane (see below).

Reliable insights on the mechanism of action and the relationships between membrane-perturbing efficacy and antibacterial activities of Drs B2 were obtained through a detailed characterization of peptide−membrane and peptide secondary and three-dimensional structures by differential scanning calorimetry, circular dichroism, and NMR spectroscopy. It is obvious that Drs B2 interacts with phospholipid bilayers in a very different manner from [1−23]-Drs B2 as inferred by DSC and CD analysis. [1−23]-Drs B2 exhibited high helical propensities when bound to anionic vesicles but had no ordered structure in the presence of zwitterionic lipids, a trend consistent with its weak perturbing activity of DMPC MLVs as demonstrated by DSC. In contrast, Drs B2 does not require the presence of anionic lipids to fold into an α-helix and has significant, but moderate perturbing effects on zwitterionic bilayers. Drs B2 had strong membrane

perturbing effects on anionic MLVs, consistent with deep penetration into the fatty acyl chains of the lipid bilayer, with formation of regions of two coexisting phases, one phase rich in peptide and the other lipid-rich. This gradual phase segregation between peptide-poor and peptide-rich domains may eventually lead to membrane disruption, thereby explaining the strong antibiotic activity of this peptide. According to the classification of Papahadjopoulos et al. and McElhaney et al. (*76, 77*), Drs B2 would thus be considered as a type II peptide which most likely resides at the hydrocarbon−water interface of the lipid bilayer, interacting with the polar head groups and glycerol backbone region of the phospholipids, and the region of the lipid acyl chain near the bilayer surface. In contrast, truncated Drs B2 resides in the lipid head group region and does not penetrate into the hydrophobic part of the bilayer, a result consistent with the biological activities of the peptide. Thus, the observation that Drs B2 perturbs more strongly anionic than zwitterionic bilayers is probably due to more favorable electrostatic and H-bonding interactions between the cationic peptide and the negatively charged surfaces of anionic bilayers. The observation that [1−23]-Drs B2 had no ordered structure when mixed with zwitterionic lipids, a trend consistent with its weak zwitterionic membrane-perturbing activity as demonstrated by DSC, is a case of unproductive binding that can reflect the low overall hydrophobicity of the peptide compared to Drs B2 (see below). Since Drs B2 and [1−23]-Drs B2 have similar positive net charges and secondary structures when bound to anionic membranes, the differences in the hydrophobic interactions of the peptides with membranes appear to be responsible for their different binding and perturbing efficacies, hence their antibacterial activities.

Placing the amino acid sequence of Drs B2 on a Schiffer−Edmunson wheel projection reveals that the peptides can adopt an amphipathic structure. The six Lys residues of Drs B2 are not clustered toward the center of the polar face of the helix but distributed around the perimeter of the polar face. In accordance with the classification scheme introduced by Segrest (*78*), Drs B2 belongs to class A amphiphatic helices, which are characterized by a large polar angle (≥180 °). The N-terminal side of the helix contains strongly hydrophobic residues Leu^2, Trp^3, Ile^6, and Val^9 that form a deep hydrophobic patch at the apolar surface of the helix. This is followed by an Ala-rich central 12−25 core that formed a shallow hydrophobic face. The C-terminal side of the helix (residues 26−33), which is shifted in orientation by ∼80° compared with the N-terminal side, demonstrates a marked amphipathic and hydrophobic character with Leu^{27}, Val^{30}, and Val^{33} constituting a second prominent hydrophobic patch at the apolar surface of the helix. This second patch is absent in [1−23]-Drs B2 due to truncation of residues 24−33 from the C-terminus of Drs B2.

Several studies have demonstrated that there are two main driving forces for the anionic membrane binding and disrupting activity of cationic, α-helical amphipathic peptides. The first is the strong electrostatic interaction between positively charged side chains of the peptide and the polar head groups of the membrane surface. The second is the partial insertion of the hydrophobic sector of the peptide helix into the acyl core of the membrane. As shown by Tossi and colleagues, the depth of the hydrophobic face of the peptide helix is one of the main factors for significant interaction and perturbation of lipid bilayers (*4*). Peptides with a shallow helical apolar face (aliphatic side chains of two carbons or less) may be unable to insert sufficiently into biological membranes so as to kill microorganisms. This suggests that the presence of two highly prominent patches of hydrophobic residues in Drs B2, one at the N-terminal side and the other at the C-terminal side of the helix, is responsible for the capacity of this peptide to structure itself helical disrespect of the net charge of the membrane and its ability to insert into and disrupt membrane bilayers. Even though [1−23]-Drs B2 had sufficient positive charge and structured adequately when bound to anionic membranes, the insufficient number of large aliphatic residues in its sequence impedes its ability to insert into and perturb anionic and zwitterionic membranes.

In terms of a mechanistic model, results from the present study strongly suggest that Drs B2 destabilizes anionic lipid bilayers through a carpet-like mechanism (*11, 27*). First, DSC results showed that Drs B2 binds to anionic membranes at the hydrocarbon−water interface with its hydrophobic sector dipping into the hydrocarbon region of the bilayer. Second, the peptide induced positive curvature in DiPoPE bilayers. Interfacial location of an amphipathic peptide produces an asymmetric perturbation in the two lipid leaflets of the bilayer and induces a spontaneous curvature stress which may lead to the formation of defects (membrane pores, peptide−micelle complexes, etc.) in the host cells. Class A peptides, such as Drs B2, are characterized by a large polar angle and insert only a small fraction of their cylinder-like bodies into the membrane, with the axis of the helix oriented parallel to the plane of the membrane. These peptides are typically found to increase the bilayer-to-hexagonal phase transition temperature in the bilayer, indicating the induction of positive curvature stress in the bilayer. On the other hand, peptides having a small polar face insert deep into the acyl core of the membrane and have opposite effect on the phase transition temperature and the curvature of the bilayer (*79*). Therefore, this suggests that Drs B2 might accumulate in the in-plane interfacial region of the outer leaflet of the membrane, where monomer−monomer interactions are weakened by the anionic lipid head groups. Once a threshold concentration is reached and/or under the influence of the transmembrane electric potential gradient, which in bacteria is about −150 mV oriented internal bilayer, a fraction of the peptide may change their orientation from parallel to perpendicular, promoting a positive curvature of the membrane and forming mixed peptide−phospholipid toroidal, transient pores (*30, 31, 41, 79, 80*).

An unexpected result of the NMR studies in SDS is that Drs B2 and [1−23]-Drs B2 adopt different structures in the presence of anionic SDS micelles. Drs B2 was found to adopt a well-defined amphipathic helix spanning residues 11−31, connected by a hinge region (Val^9-Gly^{10}) to a loosely defined helical N-terminal segment. In contrast, [1−23]-Drs B2 adopts a well-defined helix encompassing residues 2−20. Chemical shift analysis and observation of characteristic medium-range NOEs indicate that the α-helix structure does not interrupt around the Val^9-Gly^{10} pair. Thus deleting ten residues in the C-terminal part does not destabilize the helical conformation in the presence of anionic micelles. Differences in CSDs for residues 21−23 probably reflect higher flexibility

in the last turn of the helix due to peptide shortening. The large conformational changes affecting residues Val^9-Gly^{10} suggest an important role of this region in the conformational flexibility and adjustment to a membrane interface. It may be inferred that the C-terminal truncation induces different interaction modes with SDS micelle and that the Val^9-Gly^{10} segment may act as a conformational switch to adapt to a membrane environment with a high positive curvature.

What could be the relationship between the three-dimensional structure of the micelle-bound Drs B2 and the mechanism of its membrane-perturbing action? The helix−hinge−helix structural motif frequently occurs in cationic antimicrobial peptides, and structure−activity relationship studies have revealed the necessity of a hinge in magainin II, caerin 1.1, and clavanin (*81, 82*). Thus, the flexibility induced by the Val^9-Gly^{10} sequence of Drs B2 must be important in facilitating the concomitant deep insertion of the strongly hydrophobic N- and C-termini of the peptide into the acyl chains of the lipid bilayers. In contrast, because of its shorter length and the absence of a prominent hydrophobic patch at its C-terminus, [1−23]-Drs B2 needs not to kink near the Val^9-Gly^{10} flexible sequence upon binding to membrane bilayers. However, one cannot exclude that the break we observed in Drs B2 is due to the physical properties of SDS micelles. Although SDS micelles capture the essential features of negatively charged membranes, with a highly apolar core, a flexible polar interface capable of forming H-bonds and salt bridges and able to respond dynamically to peptide interactions, they have a high degree of positive surface curvature, and helices adsorbed to such surfaces are generally found to be curved. Thus, the kink observed in Drs B2 may allow the peptide to adapt to this unusual curvature strain by adopting two shorter stretches of α-helix structure.

Drs B2 was previously found to interconvert between different forms on a slow exchange time scale at high peptide concentrations (2 mM) in 80 mM SDS (*42*). Up to three distinct sets of resonances could be observed for residues in the N-terminal part, in particular, Leu^2, Trp^3, Ile^6, Lys^7, Val^9, and Gly^{10}. The amide protons of several residues (Leu^2, Val^9, Gly^{10}) were found to experience large variations (0.3−0.9 ppm) of their chemical shift between the different forms, indicating that the observed concentration-dependent equilibrium was accompanied by major conformational and environmental changes in the N-terminal segment of Drs B2. In contrast, Drs B2 was found to be monomeric at 400 μM, and only marginal effects on chemical shifts, line widths, or chemical shift heterogeneity were observed at millimolar concentrations of [1−23]-Drs B2. Thus, although the aggregating behavior of Drs B2 parallels that of Drs S4, it may not be biologically relevant since it is only observed at concentrations that are three log orders higher than the MICs of the peptide.

Finally, one may wonder why truncated natural peptides of the dermaseptin family as short as [1−18]-Drs S1 or [1−16]-Drs S3 achieve antimicrobial activity relative to [1−23]-Drs B2. For instance, Drs S1 and Drs B2 have identical positive net charge (+ 3) and similar length (34 and 33 amino acids, respectively) and exhibit 30% amino acid sequence identity. However, 8 highly hydrophobic residues (Leu, Trp, and Met) are distributed all along the sequence of [1−18]-Drs S1 and form a regular prominent hydrophobic patch at the apolar surface of the helix, as compared to [1−23]-Drs B2 in which the hydrophobic residues Leu^2, Trp^3, and Val^9 are confined within the N-terminal side of the peptide. Thus, the differences in the hydrophobic interactions of the two peptides with membranes appear to be responsible for their different binding depths in the membrane, hence their antibacterial activities.

CONCLUSION

Our results indicate that Drs B2 destabilizes anionic lipid bilayers via a positive cuvature strain and the formation of toroidal, transient pores in a way consistent with the carpet-like mechanism. They also show that the antibacterial activity of Drs B2 depends markedly on a threshold number of hydrophobic residues with chains of three or more carbon atoms to be present on both extremities of the hydrophobic apolar face of the peptide helix. Shorter aliphatic residues can be intercalated between these, but clustering of large apolar residues at only one end of the peptide helix is inefficient for antimicrobial activity. Thus, the flexibility induced by the Val^9-Gly^{10} sequence of Drs B2 must be important in facilitating the concomitant deep insertion of the strongly hydrophobic N- and C-termini of the peptide into the acyl chains of highly curved lipid bilayers.

ACKNOWLEDGMENT

We thank Dr. C. Piesse for help in synthesis and purification of peptides. We also thank Dr. Antonin Lamazière and Jessica Bois for LUV experiments.

REFERENCES

1. Bradshaw, J. P. (2003) Cationic antimicrobial peptides: issues for potential clinical use. *BioDrugs 17*, 233–240.
2. Andrès, E., and Dimarcq, J. L. (2005) Clinical development of antimicrobial peptides. *Int. J. Antimicrob. Agents 25*, 448–449.
3. Hancock, R. E., and Sahl, H. G. (2006) Antimicrobial and host-defense peptides as new anti-infective therapeutic strategies. *Nat. Biotechnol. 24*, 1551–1557.
4. Zelezetsky, I., and Tossi, A. (2006) α-Helical antimicrobial peptides: using a sequence template to guide structure-activity relationship studies. *Biochim. Biophys. Acta 1758*, 1436–1449.
5. Makovitzki, A., Avrahami, D., and Shai, Y. (2006) Ultrashort antibacterial and antifungal lipopeptides. *Proc. Natl. Acad. Sci. U.S.A. 103*, 15997–16002.
6. Conlon, J. M., Al-Ghaferi, N., Abraham, B., and Leprince, J. (2007) Strategies for transformation of naturally-occurring amphibian antimicrobial peptides into therapeutically valuable anti-infective agents. *Methods 42*, 349–357.
7. Tossi, A. Antimicrobial sequences database (http://www.bbcm.univ.trieste.it/~tossi/amsdb.html).
8. Nicolas, P., and Mor, A. (1995) Peptides as weapons against microorganisms in the chemical defense system of vertebrates. *Annu. Rev. Microbiol. 49*, 277–304.
9. Dathe, M., and Wieprecht, T. (1999) Structural features of helical antimicrobial peptides: their potential to modulate activity on model membranes and biological cells. *Biochim. Biophys. Acta 1462*, 71–87.
10. Epand, R. M., and Vogel, H. J. (1999) Diversity of antimicrobial peptides and their mechanisms of action. *Biochim. Biophys. Acta 1462*, 11–28.
11. Shai, Y. (1999) Mechanism of the binding, insertion and destabilization of phospholipid bilayer membranes by α-helical antimicrobial and cell non-selective membrane-lytic peptides. *Biochim. Biophys. Acta 1462*, 55–70.
12. Tossi, A., Sandri, L., and Giangaspero, A. (2000) Amphipathic, α-helical antimicrobial peptides. *Biopolymers 55*, 4–30.
13. Blondelle, S. E., Lohner, K., and Aguilar, M. (1999) Lipid-induced conformation and lipid binding properties of cytolytic and anti-

microbial peptides: determination and biological specificity. *Biochim. Biophys. Acta 1462*, 89–108.
14. Tochi, T., Epand, R. F., Epand, R. M., and Matsuzaki, K. (2002) Position-dependent hydrophobicity of the antimicrobial magainin peptide affects the mode of peptide-lipid interaction and selectivity. *Biochemistry 41*, 10723–10731.
15. Dathe, M., Meyer, J., Beyermann, M., Maul, B., Hoischen, C., and Bienert, M. (2002) General aspects of peptide selectivity towards lipid bilayers and cell membranes studied by variation of the structure parameters of amphipathic helical model peptides. *Biochim. Biophys. Acta 1558*, 171–186.
16. Powers, J. P., and Hancock, R. E. (2003) The relationship between peptide structure and antibacterial activity. *Peptides 24*, 1681–1691.
17. Papo, N., and Shai, Y. (2003) Can we predict biological activity of antimicrobial peptides from their interactions with model phospholipid membranes? *Peptides 24*, 1693–1703.
18. Resende, J. M., Moraes, C. M., Prates, M. V., Cesar, A., Almeida, F. C., Mundim, N. C., Valente, A. P., Bemquerer, M. P., Piló-Veloso, D., and Bechinger, B. (2008) Solution NMR structures of the antimicrobial peptides phylloseptin-1, -2, and -3 and biological activity: the role of charges and hydrogen bonding interactions instabilizing helix conformations. *Peptides 29*, 1633–1644.
19. Raimondo, D., Andreotti, G., Saint, N., Amodeo, P., Renzone, G., Sanseverino, M., Zocchi, I., Molle, G., Motta, A., and Scaloni, A. (2005) A folding-dependent mechanism of antimicrobial peptide resistance to degradation unveiled by solution structure of distinctin. *Proc. Natl. Acad. Sci. U.S.A. 102*, 6309–6314.
20. Lohner, K., and Blondelle, S. E. (2005) Molecular mechanisms of membrane perturbation by antimicrobial peptides and the use of biophysical studies in the design of novel peptide antibiotics. *Comb. Chem. High Throughput Screening 8*, 241–256.
21. Hale, J. D., and Hancock, R. E. (2007) Alternative mechanisms of action of cationic antimicrobial peptides on bacteria. *Expert Rev. Anti-Infect. Ther. 5*, 951–959.
22. Lee, M. T., Hung, W. C., Chen, F. Y., and Huang, H. W. (2008) Mechanism and kinetics of pore formation in membranes by water-soluble amphipathic peptides. *Proc. Natl. Acad. Sci. U.S.A. 105*, 5087–5092.
23. Ehrenstein, G., and Lecar, H. (1977) Electrically gated ionic channels in lipid bilayers. *Q. Rev. Biophys. 10*, 1–34.
24. Pouny, Y., Rapaport, D., Mor, A., Nicolas, P., and Shai, Y. (1992) Interaction of antimicrobial dermaseptin and its fluorescently labelled analogues with phospholipids membranes. *Biochemistry 31*, 12416–12423.
25. Matsuzaki, K. (1998) Magainins as paradigm for the mode of action of pore forming polypeptides. *Biochim. Biophys. Acta 1376*, 391–400.
26. Huang, H. W. (2000) Action of antimicrobial peptides: 2-state model. *Biochemistry 39*, 8347–8352.
27. Shai, Y. (2002) Mode of action of membrane active antimicrobial peptides. *Biopolymers 66*, 236–248.
28. Bechinger, B., and Lohner, K. (2006) Detergent-like actions of linear amphipathic cationic antimicrobial peptides. *Biochim. Biophys. Acta 1758*, 1529–1539.
29. Duclohier, H. (2002) How do channel- and pore-forming helical peptides interact with lipid membranes and how does this account for their antimicrobial activity? *Mini-Rev. Med. Chem. 2*, 331–342.
30. Aisenbrey, C., Bechinger, B., and Gröbner, G. (2008) Macromolecular crowding at membrane interfaces: adsorption and alignment of membrane peptides. *J. Mol. Biol. 375*, 376–385.
31. Jean-François, F., Elezgaray, J., Berson, P., Vacher, P., and Dufourc, E. J. (2008) Pore formation induced by an antimicrobial peptide: electrostatic effects, Biophys. J. (in press).
32. Amiche, M., Ladram, A., and Nicolas, P. (2008) A consistent nomenclature of antimicrobial peptides isolated from frogs of the subfamily Phyllomedusinae. *Peptides 29*, 2074–2082.
33. Nicolas, P., and El Amri, C. (2008) The dermaseptin superfamily: a gene-based combinatorial library of antimicrobial peptides, Biochim. Biophys. Acta (in press).
34. Mor, A., and Nicolas, P. (1994) The NH2-terminal α-helical domain 1−18 of dermaseptin is responsible for antimicrobial activity. *J. Biol. Chem. 269*, 1934–1939.
35. Savoia, D., Guerrini, R., Marzola, E., and Salvadori, S. (2008) Synthesis and antimicrobial activity of dermaseptin S1 analogues. *Bioorg. Med. Chem. 16*, 8205–8209.
36. Mor, A., Hani, K., and Nicolas, P. (1994) The vertebrate peptide antibiotics dermaseptins have overlapping structural features but target specific microorganisms. *J. Biol. Chem. 269*, 31635–31641.
37. Krugliak, M., Feder, R., Zolotarev, V. Y., Gaidukov, L., Dagan, A., Ginsburg, H., and Mor, A. (2000) Antimalarial activities of dermaseptin S4 derivatives. *Antimicrob. Agents Chemother. 44*, 2442–2451.
38. Kustanovich, I., Shalev, D. E., Mikhlin, M., Gaidukov, L., and Mor, A. (2002) Structural requirements for potent versus selective cytotoxicity for antimicrobial dermaseptin S4 derivatives. *J. Biol. Chem. 277*, 16941–16951.
39. La Rocca, P., Shai, Y., and Sansom, M. S. (1999) Peptide bilayer interactions. Simulation of dermaseptin B, an antimicrobial peptide. *Biophys. Chem. 76*, 145–169.
40. Strahilevitz, J., Mor, A., Nicolas, P., and Shai, Y. (1994) Spectrum of antimicrobial activity and assembly of dermaseptin-B and its precursor form in phospholipid membranes. *Biochemistry 33*, 10951–10960.
41. Duclohier, H. (2006) Bilayer lipid composition modulates the activity of dermaseptins, polycationic antimicrobial peptides. *Eur. Biophys. J. 35*, 401–409.
42. Lequin, O., Bruston, F., Convert, O., Chassaing, G., and Nicolas, P. (2003) Helical structure of dermaseptin B2 in a membrane-mimetic environment. *Biochemistry 42*, 10311–10323.
43. Shalev, D. E., Mor, A., and Kustanovich, I. (2002) Structural consequences of carboxyamidation of dermaseptin S3. *Biochemistry 41*, 7312–7317.
44. Feder, R., Dagan, A., and Mor, A. (2000) Structure-activity relationship study of antimicrobial dermaseptin S4 showing the consequences of peptide oligomerization on selective cytotoxicity. *J. Biol. Chem. 275*, 4230–4238.
45. Jean-François, F., Castano, S., Desbat, B., Odaert, B., Roux, M., Metz-Boutigue, M. H., and Dufourc, E. J. (2008) Aggregation of cateslytin beta-sheets on negatively charged lipids promotes rigid membrane domains. A new mode of action for antimicrobial peptides? *Biochemistry 47*, 6394–6402.
46. Auvynet, C., El Amri, C., Lacombe, C., Bruston, F., Bourdais, J., Nicolas, P., and Rosenstein, Y. (2008) Structural requirements for antimicrobial versus chemoattractant activities for dermaseptin S9. *FEBS J. 275*, 4134–4151.
47. Abbassi, F., Oury, B., Blasco, T., Sereno, D., Bolbach, G., Nicolas, P., Hani, K., Amiche, M., and Ladram, A. (2008) Isolation, characterization and molecular cloning of new temporins from the skin of the North African ranid Pelophylax saharica. *Peptides 29*, 1526–1533.
48. Vanhoye, D., Bruston, F., Nicolas, P., and Amiche, M. (2003) Antimicrobial peptides from hylid and ranin frogs originated from a 150-million-year-old ancestral precursor with a conserved signal peptide but a hypermutable antimicrobial domain. *Eur. J. Biochem. 270*, 2068–2081.
49. Lamaziere, A., Wolf, C., Lambert, O., Chassaing, G., Trugnan, G., and Ayala-Sanmartin, J. (2008) The homeodomain derived peptide Penetratin induces curvature of fluid membrane domains. *PLoS ONE 3*, e1938.
50. Lamaziere, A., Burlina, F., Wolf, C., Chassaing, G., Trugnan, G., and Ayala-Sanmartin, J. (2007) Non-metabolic membrane tubulation and permeability induced by bioactive peptides. *PLoS ONE 2*, e201.
51. Abbassi, F., Galanth, C., Amiche, M., Saito, K., Piesse, C., Zargarian, L., Hani, K., Nicolas, P., Lequin, O., and Ladram, A. (2008) Solution structure and model membrane interactions of temporins-SH, antimicrobial peptides from amphibian skin. A NMR spectroscopy and differential scanning calorimetry study. *Biochemistry 47*, 10513–10525.
52. Bruston, F., Lacombe, C., Zimmermann, K., Piesse, C., Nicolas, P., and El Amri, C. (2007) Structural malleability of plasticins: preorganized conformations in solution and relevance for antimicrobial activity. *Biopolymers 86*, 42–56.
53. Rucker, S. P., and Shaka, A. J. (1989) Broadband homonuclear cross polarization in 2D NMR using DIPSI-2. *Mol. Phys. 58*, 509–517.
54. Sklenar, V., Piotto, M., Leppik, R., and Saudek, V. (1993) Gradient-tailored water suppression for proton-nitrogen-15 HSQC experiments optimized to retain full sensitivity. *J. Magn. Reson. A 102*, 241–245.
55. Lippens, G., Dhalluin, C., and Wieruszeski, J. M. (1995) Use of a water flip-back pulse in the homonuclear NOESY experiment. *J. Biomol. NMR 5*, 327–331.
56. Dhalluin, C., Wieruszeski, J. M., and Lippens, G. (1996) An improved homonuclear TOCSY experiment with minimal water saturation. *J. Magn. Reson. B 111*, 168–170.

57. Grzesiek, S., and Bax, A. (1993) The importance of not saturating H_2O in protein NMR. Application to sensitivity enhancement and NOE measurements. *J. Am. Chem. Soc. 115*, 12593–12594.
58. Schleucher, J., Schwendinger, M., Sattler, M., Schmidt, P., Schedletzky, O., Glaser, S. J., Sorensen, O. W., and Griesinger, C. (1994) A general enhancement scheme in heteronuclear multidimensional NMR employing pulsed field gradients. *J. Biomol. NMR 4*, 301–306.
59. Bartels, C., Xia, T. H., Billeter, M., Güntert, P., and Wüthrich, K. (1995) The program XEASY for computer-supported NMR spectral analysis of biological macromolecules. *J. Biomol. NMR 6*, 1–10.
60. Wishart, D. S., Bigam, C. G., Holm, A., Hodges, R. S., and Sykes, B. D. (1995) ^{1}H, ^{13}C and ^{15}N random coil NMR chemical shifts of the common amino acids. I. Investigations of nearest-neighbor effects. *J. Biomol. NMR 5*, 67–81.
61. Szyperski, T., Güntert, P., Otting, G., and Wüthrich, K. (1992) Determination of scalar coupling constants by inverse Fourier transformation of in-phase multiplets. *J. Magn. Reson. 99*, 552–560.
62. Cornilescu, G., Delaglio, F., and Bax, A. (1999) Protein backbone angle restraints from searching a database for chemical shift and sequence homology. *J. Biomol. NMR 13*, 289–302.
63. Güntert, P., Mumenthaler, C., and Wüthrich, K. (1997) Torsion angle dynamics for NMR structure calculation with the new program DYANA. *J. Mol. Biol. 273*, 283–298.
64. Schwieters, C. D., Kuszewski, J. J., Tjandra, N., and Clore, M. G. (2003) The Xplor-NIH NMR molecular structure determination package. *J. Magn. Reson. 160*, 65–73.
65. Laskowski, R. A., Rullmannn, J. A., MacArthur, M. W., Kaptein, R., and Thornton, J. M. (1996) AQUA and PROCHECK-NMR: programs for checking the quality of protein structures solved by NMR. *J. Biomol. NMR 8*, 477–486.
66. Zhang, Y. P., Lewis, R. N. A. H., and McElhaney, R. N. (1997) Calorimetric and spectroscopic studies of the thermotropic phase behavior of the n-saturated 1,2-diacylphosphatidylglycerols. *Biophys. J. 72*, 779–793.
67. Suezaki, Y., Tatara, T., Kaminoh, Y., Kamaya, H., and Ueda, I. (1990) A solid-solution theory of anesthetic interaction with lipid membranes: temperature span of the main phase transition. *Biochim. Biophys. Acta 1029*, 143–148.
68. McElhaney, R. N. (1986) Differential scanning calorimetric studies of lipid-protein interactions in model membrane systems. *Biochim. Biophys. Acta 864*, 361–421.
69. Lohner, K., and Prenner, E. J. (1999) Differential scanning calorimetry and X-ray diffraction studies of the specificity of the interaction of antimicrobial peptides with membrane-mimetic systems. *Biochim. Biophys. Acta 1462*, 141–156.
70. Henzler-Wildman, K. A., Martinez, G. V., Brown, M. F., and Ramamoorthy, A. (2004) Perturbation of the hydrophobic core of lipid bilayers by the human antimicrobial peptide LL-37. *Biochemistry 43*, 8459–8469.
71. Seto, G. W. J., Marwaha, S., Kobewka, D. M., Lewis, R. N., Separovic, F., and McElhaney, R. N. (2007) Interactions of the Australian tree frog antimicrobial peptides aurein 1.2, citropin 1.1 and maculatin 1.1 with lipid model membranes: differential scanning calorimetric and Fourier transform infrared spectroscopic studies. *Biochim. Biophys. Acta 1768*, 2787–2800.
72. Hallock, K. J., Lee, D. K., and Ramamoorthy, A. (2003) MSI-78, an analogue of the magainin antimicrobial peptides, disrupts lipid bilayer structure via positive curvature strain. *Biophys. J. 84*, 3052–3060.
73. El Amri, C., Lacombe, C., Zimmerman, K., Ladram, A., Amiche, M., Nicolas, P., and Bruston, F. (2006) The plasticins: membrane adsorption, lipid disorders, and biological activity. *Biochemistry 44*, 14285–14297.
74. Abraham, T., Marwaha, S., Kobewka, D. M., Lewis, R. N. A. H., Prenner, E. J., Hodges, R. S., and McElhaney, R. N. (2007) The relationship between the binding to and permeabilization of phospholipid bilayer membranes by GS14dK4, a designed analog of the antimicrobial peptide gramicidin S. *Biochim. Biophys. Acta 1768*, 2089–2098.
75. Liu, F., Lewis, R. N. A. H., Hodges, R. S., and McElhaney, R. N. (2004) Effect of variations in the structure of polyleucine-based α-helical transmembrane peptide on its interaction with phosphatidylethanolamine bilayers. *Biophys. J. 87*, 2470–2482.
76. Papahadjopoulos, D., Moscarello, M., Eylar, E. H., and Isac, T. (1975) Effects of proteins on thermotropic phase transitions of phospholipid membranes. *Biochim. Biophys. Acta 401*, 317–335.
77. McElhaney, R. N. (1982) The use of differential scanning calorimetry and differential thermal analysis in studies of model and biological membranes. *Chem. Phys. Lipids 30*, 229–259.
78. Segrest, J. P., Garber, D. W., Brouillette, C. G., Harvey, S. C., and Ananthraramaiah, G. M. (1994) The amphipathic α helix: a multifunctional structural motif in plasma apolipoproteins. *Adv. Protein Chem. 45*, 303–369.
79. Zemel, A., Ben-Shaul, A., and May, S. (2008) Modification of the spontaneous curvature and bending rigidity in lipid membranes by interfacially adsorbed amphipathic peptides. *J. Phys. Chem. 112*, 6988–6996.
80. Campagna, S., Saint, N., Molle, G., and Aumelas, A. (2007) Structure and mechanism of action of the antimicrobial peptide piscidin. *Biochemistry 46*, 1771–1778.
81. Pukala, T. L., Brinkworth, C. S., Carver, J. A., and Bowie, J. H. (2004) Investigating the importance of the flexible hinge in caerin 1.1: solution structures and activity of two synthetically modified caerin peptides. *Biochemistry 43*, 937–944.
82. van Kan, E. J., van der Bent, A., Demel, R. A., and de Kruijff, B. (2001) Membrane activity of the peptide antibiotic clavanin and the importance of its glycine residues. *Biochemistry 40*, 6398–6405.

BI802025A